Supplementary Material

Improved siRNA Delivery Efficiency via Solvent-Induced Condensation of Micellar Nanoparticles

Juan Wu,[1†] Wei Qu,[2 †] John-Michael Williford,[3,4 †] Yong Ren,[1,4] Xuesong Jiang,[1,5] Xuan Jiang,[1] Deng Pan,[3] Hai-Quan Mao,[1,4,5 *] and Erik Luijten[2,6 **]

[1]Department of Materials Science and Engineering,
Johns Hopkins University, Baltimore, MD 21218

[2]Department of Materials Science and Engineering,
Northwestern University, Evanston, Illinois 60208

[3]Department of Biomedical Engineering,
Johns Hopkins School of Medicine, Baltimore, Maryland 21205

[4]Institute for NanoBioTechnology,
Johns Hopkins University, Baltimore, MD 21218

[5]Translational Tissue Engineering Center and Whitaker Biomedical Engineering Institute,
Johns Hopkins School of Medicine, Baltimore, Maryland 21287

[6]Department of Engineering Sciences and Applied Mathematics,
Northwestern University, Evanston, Illinois 60208

*hmao@jhu.edu

**luijten@northwestern.edu

[†]These authors contributed equally to this work.

1. Experimental Methods

1.1. Synthesis and characterization of lPEI-g-PEG copolymer

A PEGylated linear PEI (lPEI) copolymer, lPEI-g-PEG, was synthesized by grafting 10 kDa PEG to lPEI with an average M_n of 17 kDa. We chose lPEI owing to its lower cytotoxicity compared to branched PEI [1] and selected lPEI of relatively high M_n for its higher siRNA condensation capacity and transfection efficiency compared to lPEI of lower molecular weight [2]. The 10 kDa PEG grafts were chosen based upon their ability to provide more effective resistance to protein adsorption and better protection against nuclease degradation than PEG of lower molecular weight [3, 4].

Linear polyethyleneimine HCl salt (lPEI·HCl, M_n = 17 kDa) was purchased from Polymer Chemistry Innovations, Inc. (Tucson, AZ). *N*-hydroxysuccinimidyl ester of methoxy polyethylene glycol hexanoic acid (PEG-NHS, M_n = 10 kDa) was purchased from NOF America Corporation (White Plains, NY). The lPEI·HCl (7.95 mg, 0.1 mmol of amine) was dissolved in 1 mL of DI water. The pH of the solution was adjusted to 6 through drop-wise addition of 1 M NaOH solution. The solution was then mixed with 80 mg of PEG-NHS and incubated overnight. The reaction mixture was dialyzed against DI water and lyophilized to yield a white foam-like solid with a 95% yield. The molecular weight of the graft copolymer was characterized by gel permeation chromatography using an Agilent 1200 series Isocratic HPLC System equipped with TSKgel G3000PWxl-CP column and TSKgel G5000PWxl-CP column (Tosoh America, Inc., Grove City, OH), which was connected to a multi-angle light-scattering detector (MiniDawn, Wyatt Technology, Santa Barbara, CA). The grafting degree of PEG on lPEI was found to be 1.2%, which corresponds to an average of 4.6 PEG grafts per lPEI.

1.2. Gel electrophoresis analysis of polycation/siRNA nanoparticles

To investigate polycation/siRNA condensation, equal volumes of polymer and siRNA solution were mixed at increasing N/P ratios (molar ratio of amine in lPEI to phosphate in RNA) followed by electrophoresis at 90 V for 40 min on a 1.2 wt% agarose gel. To determine siRNA release from uncrosslinked and crosslinked particles, 20 μM sodium dextran sulfate (M_n = 200 kDa) in 10 mM Tris-HCl (pH 7.4) buffer was added to equal volume of nanoparticle solution containing 1 μM siRNA. The mixed solution was further incubated in the presence or

absence of 50 mM DTT overnight at 37°C. An aliquot of each sample was then subjected to electrophoresis as above. The siRNA bands were visualized under a UV transilluminator. **Figure S1** displays the gel retardation analysis, confirming that a minimum N/P ratio of 20 is needed to completely condense siRNA under the tested conditions.

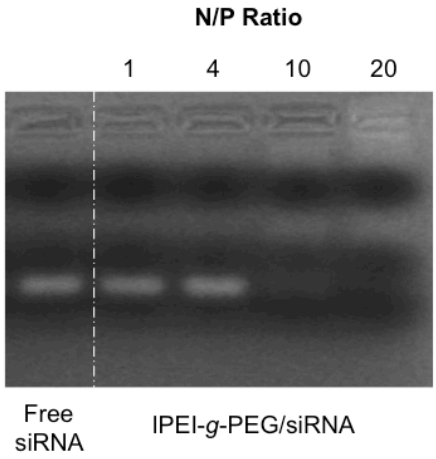

Figure S1. Gel retardation assay of complexation between lPEI-*g*-PEG and siRNA at increasing N/P ratios. Note the faint siRNA band for an N/P ratio of 10.

1.3. Transmission electron microscopy (TEM)

Samples were prepared by depositing 10 μL nanoparticle solution on a freshly ionized nickel grid covered by a carbon film. After 10 min, excess liquid was removed by pipetting. A drop of 2% uranyl acetate solution (~5 μL) was then deposited on the grid for 10 s and subsequently removed. After drying at room temperature, the samples were examined on a Tecnai FEI-12 electron microscope.

1.4. Preparation of crosslinked lPEI-g-PEG/siRNA nanoparticles

lPEI-*g*-PEG copolymer was thiolated with Traut's reagent at a 20% grafting degree of the total amino groups for 2 h at room temperature. The thiolated polymer solution was mixed with siRNA, and the micelle solution was transferred to a dialysis membrane with MWCO of 3.5 kDa and then subjected to aerial oxidation for 48 h with stirring to crosslink the micelles. Following the assembly and crosslinking steps, the nanoparticles were purified by removing DMF and other small molecular agents through dialysis against water for 24 h with frequent change of water.

1.5. Nanoparticle size and zeta potential measurements

Particle size and zeta potential were measured by photon correlation spectroscopy and laser Doppler anemometry, respectively, using a Zetasizer Nano ZS90 (Malvern Instruments, Southborough, MA). Size measurement was performed at 25°C at a 90° scattering angle. The mean hydrodynamic diameter was determined by cumulative analysis. The zeta potential measurements were performed using a DTS1060-folded capillary cell in the automatic mode. **Figure S2** reveals the average zeta potential of lPEI-*g*-PEG/siRNA micelles before and after crosslinking, revealing a decrease in particle zeta potential from +5 mV to –5 and –8 mV for 117 nm and 44 nm particles, respectively.

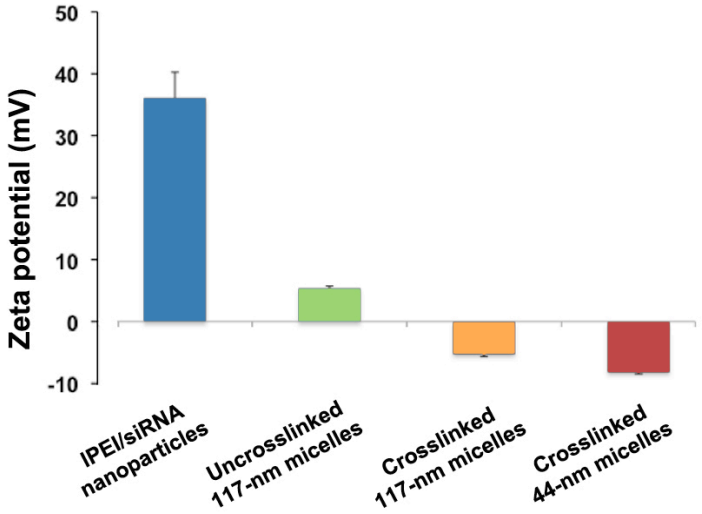

Figure S2. Zeta potential of lPEI-*g*-PEG/siRNA micelles before crosslinking and after crosslinking in both DI water and 7:3 (v/v) DMF–water mixture. Bars show mean ± SD (n = 3).

1.6. Characterization of in vitro gene knockdown efficiency

For gene silencing *in vitro*, cells were pre-transfected with 720 ng/well pGL3 DNA, encoding for firefly luciferase, and 80 ng/well pRL-CMV, encoding for Renilla luciferase, using Lipofectamine 2000 according to our previously published protocol. After 4 h, cells were transfected with nanoparticles carrying GL3 siRNA
(sense strand 5'-CUUACGCUGAGUACUUCGAdTdT-3',
antisense strand 5'-UCGAAGUACUCAGCGUAAGdTdT-3'),

or a negative control sequence (AllStars Neg. siRNA, Qiagen, Valencia, CA) at a dose equivalent to 100 nM siRNA. After 48 h, cells were rinsed with PBS and assayed for luciferase expression using a dual luciferase reporter assay kit (Promega, WI). For each well, firefly and Renilla luciferase luminescence was measured using a FLUOstar OPTIMA plate reader (BMG Labtech, Germany). Firefly readings were normalized against Renilla readings, and values were expressed as a ratio to the untreated control.

1.7. Characterization of cytotoxicity of polycation/siRNA nanoparticles

Cytotoxicity of siRNA nanoparticles was determined by a WST-1 dye reduction assay. HepG2 cells were seeded in a 96-well plate 24 h before assay at a density of 20,000 cells/well. The cells were incubated for 4 h with 100 μL complete medium containing nanoparticles at a dose equivalent to 100 nM of siRNA. The medium in each well was then replaced with 100 μL fresh medium containing 10 μL WST-1 reagent (Roche, Mannheim, Germany). The cells were incubated for 1 h at 37°C. The absorbance of the supernatant at 450 nm, using 600 nm as a reference wavelength, was measured on a microplate reader (Infinite M200, TECAN, Männedorf, Switzerland). **Figure S3** illustrates the metabolic activity of HepG2 cells that were treated with different formulations of lPEI-*g*-PEG/siRNA micelles. All formulations maintained >80% cell viability at the tested concentrations.

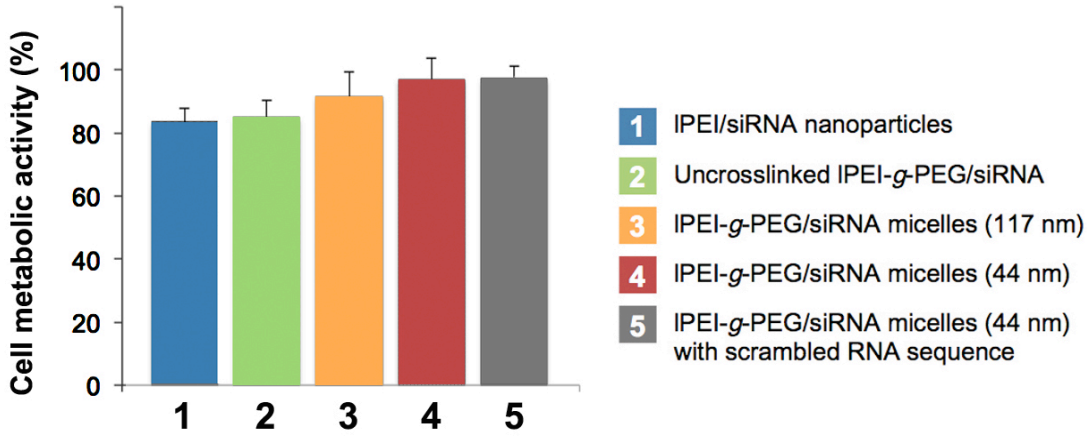

Figure S3. Metabolic activities of HepG2 cells treated with lPEI-*g*-PEG/siRNA micelles at a dose equivalent to 100 nM siRNA. Bars show mean ± SD (n = 4).

2. Computational Methods

2.1. Simulation model and coarse-graining procedure

Molecular dynamics simulations were performed using the LAMMPS package [5]. The large length and time scales involved in micelle formation make it essential to employ coarse-grained models of lPEI, lPEI-*g*-PEG copolymer, and siRNA. The Bjerrum length in water is 7.1 Å, which was chosen as the Lennard-Jones (LJ) unit of distance σ in our simulations. Since lPEI and PEG share a similar molecular structure, we treated them equivalently in the coarse-graining procedure and adopted the same monomer length of 3.5 Å and intrinsic persistence length of 3.8 Å [6, 7]. Three persistence length units were represented as one bead in the model. Based on the blob concept, each bead has a size of approximately 1σ (size of blob $\approx 3^{0.6} \times 3.8$ Å = 7.35 Å ≈ σ). Clearly, for such short segments, the scaling behavior of a long self-avoiding polymer does not fully apply. Nonetheless, this coarse-graining procedure provides a consistent approach to estimate the length of the coarse-grained polymer models for our simulation (*cf.* **Table S1**).

Structural Parameter	PEG	lPEI
Molecular weight (g/mol)	9,500	17,000
Number of monomers	225	386
Number of persistence length segments*	207	356
Number of beads in coarse-grained model*	69	119

Table S1. Molecular weights of PEG and lPEI used in experiments and number of beads in coarse-grained PEG and lPEI models used in simulations. (*Assuming lPEI and PEG have the same persistence length and the same monomer size.)

For lPEI, we used a charge density of approximately 35% [8], corresponding to a pH of 6–7, as used in the experiments. The charges were evenly distributed along the model beads and each bead carried a charge of 1.12*e* (this includes a factor 3.8/3.5 to account for the ratio between persistence length and monomer size). The siRNA molecule was coarse-grained using the VMD Shape-Based Coarse-Graining (SBCG) tool [9, 10], which approximates the shape of a molecule

using a specified number of beads, and outputs the positions of each bead, the equilibrium bond length between beads, and the charge on each bead. Although the SBCG tool produces a (narrow) distribution of bead sizes, we opted for beads of uniform size σ (7.1 Å) to avoid inhomogeneous short-range and electrostatic interactions (the LJ radius of beads affects the contact strength of their electrostatic interaction as well as the range of their LJ interaction). This uniformity was achieved by adjusting the number of coarse-grained beads until the average bead size was close to 7.1 Å, and then setting all beads to this uniform size. For the coarse graining of siRNA, we isolated a 22 bp RNA molecule from the Protein Data Bank file 2F8S [11] and coarse-grained it into a 24-bead rigid body.

In the coarse-grained models, all harmonic interactions were represented by

$$U_{\text{bond}} = 200\varepsilon\left(r - r_0\right)^2 , \tag{1}$$

where r is the center-to-center distance between two bonded beads and r_0 is the equilibrium bond length, with ε the LJ unit of energy. For lPEI and PEG, r_0 was set to 1.12σ; for siRNA r_0 was determined by the SBCG coarse-graining procedure. The electrostatic energies and forces were computed using the Particle–Particle Particle–Mesh Ewald algorithm, with a relative accuracy of 10^{-4}.

Even when these coarse-grained models were employed, it was still impractical to efficiently simulate the experimental system, owing to the strong multi-chain aggregation and the slow conformational decorrelation of long polymer chains. To overcome these limitations, it was necessary to decrease the length of the polymer chains. We therefore scaled down each original coarse-grained model to one fourth of its original length, using 30 beads to represent lPEI, 15 beads to represent a PEG block, and six beads (four carrying a charge $-1.8e$ and two carrying a charge $-1.9e$) to represent siRNA. As an additional benefit, this made it possible to simulate a system with a larger number of constituent particles, namely 32 lPEI or lPEI-*g*-PEG polymers and 96 siRNA, thus permitting a better resolution of the aggregate size distribution function. In addition, 1056 positive and 1075 negative monovalent counterions were included to maintain system charge neutrality (1 additional counterion with charge $-0.2e$ was added to ensure precise electroneutrality).

We employed a Langevin thermostat to simulate the implicit solvent and control the temperature, imposing a damping time 100τ, where τ is the LJ unit of time,

$$\tau = \sqrt{\frac{m\sigma^2}{\varepsilon}} \ , \qquad (2)$$

with m the LJ unit of mass. The equations of motion were integrated using the velocity-Verlet algorithm. The (reduced) temperature was set to $T = 1.0\ \varepsilon/k_B$, where k_B is Boltzmann's constant. When the solvent is changed from pure water to DMF–water mixtures at different proportions, the dielectric constant increases, while the charge density of siRNA and lPEI polymers decreases. Following our previous work [12], we exploited the approximate cancellation of these effects in the electrostatic interaction strength and assumed a constant Bjerrum length and constant charge density in our model.

2.2. Parameter choices to represent solvent quality and hydrogen bonding

Linear PEI forms a crystal hydrate in pure water due to strong inter- and intra-molecular hydrogen bonding [13]. DMF was observed in experiments to be a good solvent for lPEI [14]. On the other hand, as the solvent is changed from pure water to DMF–water mixture, the solvent quality for siRNA decreases. Since we employed an implicit solvent, the change from a good to a poor solvent was represented by an increase in the effective attraction between siRNA beads and between lPEI beads. Since the lPEI and siRNA already experience a strong electrostatic attraction, no additional solvent-induced effective attraction between lPEI and siRNA was imposed. Both water and DMF and their mixtures are good solvents for PEG [15], therefore, following our earlier study [12], we did not incorporate PEG solubility variations within the range of DMF/water ratios in our model, but instead represented the uniformly good solvent conditions for PEG *via* a purely repulsive shifted-truncated LJ potential with a cutoff $2^{1/6}\sigma$.

In the coarse-grained modeling, we aimed to elucidate the effect of variation of the solvent quality and the degree of hydrogen bonding on the experimental system, rather than to realize a precise mapping between different solvent conditions onto attractive pair potentials. Thus, we opted to describe the pair potential *via* a LJ potential with two different strengths: 1.0 k_BT and 0.314 k_BT. A potential strength of 1.0 k_BT represented a poor-solvent condition and a higher level of polymer–polymer hydrogen bonding (which includes both direct hydrogen bonding between two monomers and hydrogen bond bridging between two monomers by water molecules); a LJ attraction of 0.314 k_BT (corresponding to the theta solvent condition for the bead–spring model employed [16]) indicated a relatively good solvent condition and a lower level of polymer–

polymer hydrogen bonding. This approach allowed us to identify the relative effect of each of the interactions during the solvent change. Given our choice for the temperature, this yielded the parameter combinations listed in **Table S2**. The pair potential was cut off at 2.5σ and shifted at the cutoff to eliminate a discontinuity in the interaction. All other non-bonded short-range interactions were modeled with a purely repulsive shifted-truncated LJ potential with a cutoff of $2^{1/6}\sigma$.

Solvent Condition	ε_{LJ} / ε (siRNA)	ε_{LJ} / ε (PEI)	ε_{LJ} / ε (PEI–PEG)
Solvent 1 (Water)	0.314	1.000	1.000
Solvent 2 (DMF–water mixture)	1.000	0.314	0.314
Solvent 1*	0.314	1.000	0.314

Table S2. Effective attraction strength ε_{LJ} (in units of the LJ energy parameter ε) between siRNA beads, PEI beads, and between lPEI and PEG beads for different solvent conditions.

To test the effect of hydrogen bonding between lPEI and PEG on micelle size, we artificially weakened the interaction strength between lPEI and PEG in water (cf. main text) and labeled this solvent condition Solvent 1*. The size distribution of lPEI-*g*-PEG nanoparticles in Solvent 1* is shown in **Fig. S4**, along with the size distribution of the same system in Solvent 1 as a comparison. Figure S4 clearly shows that without strong hydrogen bonding between lPEI and PEG, the micelles decrease in size.

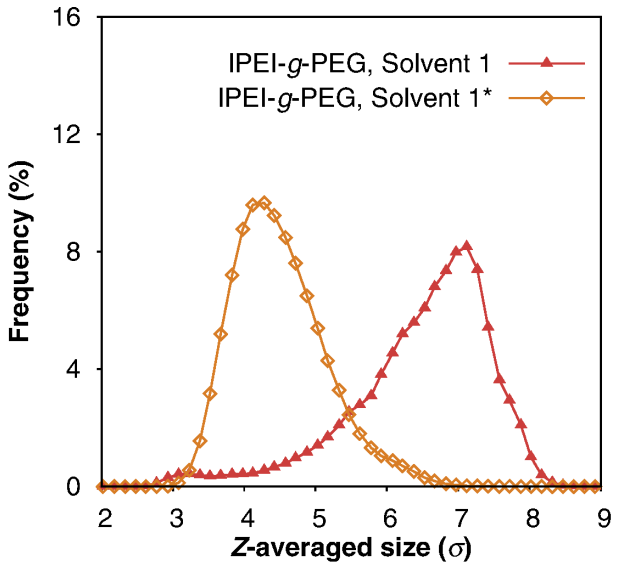

Figure S4. Size distributions of lPEI-*g*-PEG nanoparticles in Solvent 1, with strong lPEI–PEG hydrogen bonding (Solvent 1) and artificially weakened lPEI–PEG hydrogen bonding (Solvent 1*). See Table S2 for simulation parameters.

To confirm the qualitative validity of our parameter choices we also compared the experimental and computational results for the effect of solvent composition on lPEI/siRNA nanoparticles. **Figure S5** shows that for lPEI/siRNA systems, the proposed simulation model with the two-state solvent parameters successfully captured the experimentally observed size variation. As the solvent is changed from pure water to a 7:3 (v/v) DMF–water mixture, the solvent quality for lPEI increases and that for siRNA decreases. Although the two solvent effects change in opposing directions, the lPEI solubility dominates in the complexation of lPEI/siRNA, as demonstrated by the larger particle size in water and the smaller particle size in DMF–water mixture (*cf.* Fig. S5). This behavior can be ascribed to the more flexible backbone and the larger contour length of lPEI, which leads to more lPEI–solvent contacts, whereas the siRNA predominantly aggregates *via* lPEI-mediated contacts.

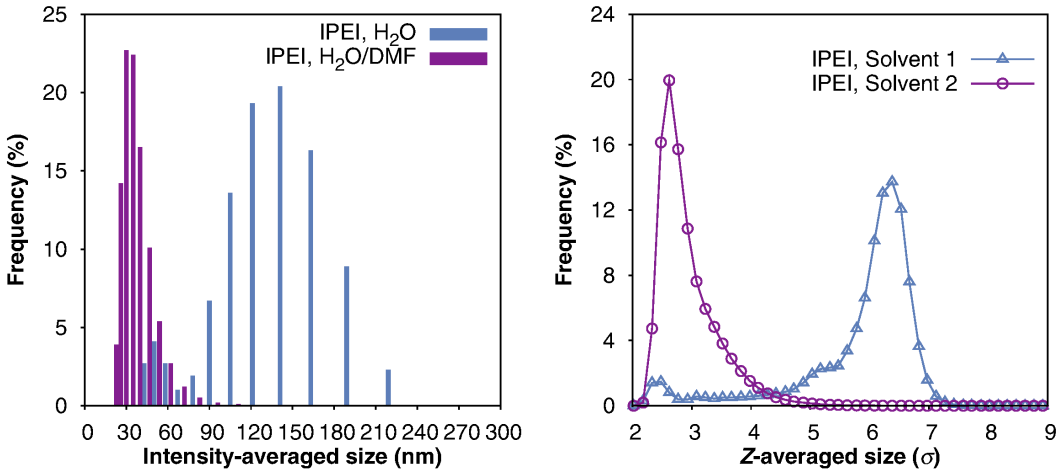

Figure S5. Size distributions of lPEI/siRNA nanoparticles in water and in 7:3 (v/v) DMF–water mixture in experiment (left) and in Solvent 1 and Solvent 2, respectively, in simulations (right).

2.3. Equilibration in the simulations and the use of parallel tempering

The siRNA molecules, the lPEI-*g*-PEG copolymers/lPEI polymers and the counterions were initially placed in a cubic, periodically replicated simulation box with linear size 100σ. To achieve a random initial configuration, a shifted and truncated LJ interaction with cutoff $2^{1/6}\,\sigma$ was used as the only pairwise interaction between any two particles. After an equilibration period of $3 \times 10^3\,\tau$ with time step 0.01τ, the proper LJ interactions (as described above) and all electrostatic interactions were switched on, followed by a second equilibration period of 1200τ. Due to the strong multi-chain attractions, in a typical simulation aggregates only seldom broke up and reformed, making it difficult to obtain an accurate frequency distribution of the aggregate size. To accelerate the dissociation and reformation of aggregates, we therefore employed the parallel tempering method [17]. In this approach, 24 copies of the same system were simulated in parallel, at different temperatures that were logarithmically distributed between $1.0\,k_BT$ and $2.0\,k_BT$. An exchange between configurations simulated at adjacent temperatures was attempted every 200 steps. This approach exploits the larger degree of fluctuations at higher temperatures to provide a pathway for the simulations at the original temperature to transition between states that are separated by high free-energy barriers. Four to eight parallel tempering runs were performed for each solvent condition, each for a period of $4.8 \times 10^5\,\tau$ (corresponding to 10–20

days of CPU time for each of the 24 parallel copies, depending on solvent condition). Following the first two equilibration stages, complexation was permitted to proceed for $6 \times 10^4 \tau$ before sampling was started.

2.4. Determination of the aggregate composition and size distribution in simulation

The nanoparticles or micelles are aggregates of siRNA and lPEI or lPEI-*g*-PEG predominantly bound by electrostatic interactions. To determine the composition of one aggregate, we first determined all the RNA molecules associated with an lPEI or lPEI-*g*-PEG polymer. If one of the siRNA beads (which were all negatively charged) was within a distance 2σ from an lPEI bead (which were all positively charged), the siRNA was considered to be associated with that lPEI or lPEI-*g*-PEG chain. We then identified all the lPEI or lPEI-*g*-PEG polymers that were sharing at least one siRNA, and assigned all the polymers and siRNA molecules associated with each of the polymers to one aggregate.

Experimentally, the particle size distribution was determined by DLS, and reported as the intensity-averaged distribution of the hydrodynamic diameter of the particles. The hydrodynamic diameter obtained by DLS is calculated based on the diffusion coefficient of the particle in the solvent. For lPEI-*g*-PEG/siRNA nanoparticles, the PEG blocks are able to affect the diffusion behavior of the particles and thereby contribute to the hydrodynamic diameter of the particles. Therefore, in simulation, we included the contribution from PEG blocks in the particle-size calculation. As the intensity-averaged size distribution can be approximated by the *z*-averaged size distribution when the single-particle scattering factor is set to unity [18], we calculated the *z*-averaged radius of gyration R_z,

$$R_Z = \frac{\sum_i N_i M_i^2 R_i}{\sum_i N_i M_i^2} \quad , \tag{3}$$

in which N_i is the number of micelles of radius of gyration R_i and mass M_i.

Although the PEG blocks are included in this size calculation, one advantage of simulation lies in the flexibility of data analysis. In **Fig. S6**, we re-analyzed the size distribution data shown in Fig. 1D, and compared the particle size with and without considering the PEG blocks. For Solvent 1, the PEG blocks were found to only contribute to a small increase in the size of lPEI-*g*-PEG/siRNA nanoparticles. If the PEG blocks were not included, the calculated size of the

nanoparticles decreased to an average similar to that of the lPEI/siRNA nanoparticles (Fig. S5), but with a different distribution, suggesting that the size increase in Figs. 1A and 1B should not be ascribed to the inclusion of PEG blocks alone. On the other hand, for Solvent 2 the PEG blocks contributed greatly to the calculated size increase of lPEI-*g*-PEG/siRNA micelles, due to the fact that the higher solubility of lPEI yielded a less compact core with a more diffuse PEG corona.

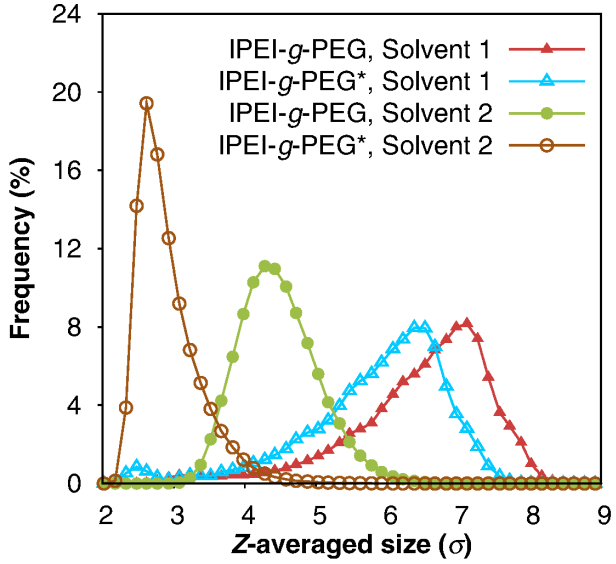

Figure S6. Size distributions of nanoparticles in Solvent 1 and Solvent 2 from simulations. In addition to the distributions of Fig. 1D, two size distributions for lPEI-*g*-PEG/siRNA nanoparticles in Solvent 1 and Solvent 2 are shown, for which PEG blocks are not included in the size calculation (labeled by lPEI-*g*-PEG*). See supplementary text for discussion.

Supplementary References

1. Jere, D., et al., *Degradable polyethylenimines as DNA and small interfering RNA carriers.* Expert Opin Drug Deliv, 2009. **6**(8): p. 827-34.
2. Grayson, A.C.R., A.M. Doody, and D. Putnam, *Biophysical and structural characterization of polyethylenimine-mediated siRNA delivery in vitro.* Pharm Res, 2006. **23**(8): p. 1868-1876.
3. Gref, R., et al., *'Stealth' corona-core nanoparticles surface modified by polyethylene glycol (PEG): influences of the corona (PEG chain length and surface density) and of the core composition on phagocytic uptake and plasma protein adsorption.* Colloids Surf B Biointerfaces, 2000. **18**(3-4): p. 301-313.
4. Mao, S., et al., *Influence of polyethylene glycol chain length on the physicochemical and biological properties of poly(ethylene imine)-graft-poly(ethylene glycol) block copolymer/SiRNA polyplexes.* Bioconjug Chem, 2006. **17**(5): p. 1209-1218.
5. Plimpton, S., *Fast Parallel Algorithms for Short-Range Molecular Dynamics.* J Comput Phys, 1995. **117**(1): p. 1–19.
6. Hansen, P.L., et al., *Osmotic Properties of Poly(Ethylene Glycols): Quantitative Features of Brush and Bulk Scaling Laws.* Biophys J, 2003. **84**(1): p. 350-355.
7. Kienberger, F., et al., *Static and Dynamical Properties of Single Poly(Ethylene Glycol) Molecules Investigated by Force Spectroscopy.* Single Molecules, 2000. **1**(2): p. 123-128.
8. Lindquist, G.M. and R.A. Stratton, *The role of polyelectrolyte charge density and molecular weight on the adsorption and flocculation of colloidal silica with polyethylenimine.* J Colloid Interface Sci, 1976. **55**(1): p. 45-59.
9. Arkhipov, A., P.L. Freddolino, and K. Schulten, *Stability and Dynamics of Virus Capsids Described by Coarse-Grained Modeling.* Structure, 2006. **14**(12): p. 1767-1777.
10. Arkhipov, A., Y. Yin, and K. Schulten, *Four-Scale Description of Membrane Sculpting by BAR Domains.* Biophys J, 2008. **95**(6): p. 2806-2821.
11. Yuan, Y.-R., et al., *A Potential Protein-RNA Recognition Event along the RISC-Loading Pathway from the Structure of A. aeolicus Argonaute with Externally Bound siRNA.* Structure, 2006. **14**(10): p. 1557-1565.
12. Jiang, X., et al., *Plasmid-Templated Shape Control of Condensed DNA-Block Copolymer Nanoparticles.* Adv Mater, 2013. **25**(2): p. 227-232.
13. Gembitskii, P.A., et al., *Properties of linear polyethylene imine and its oligomers.* Polymer Science USSR, 1978. **20**(11): p. 2932-2940.
14. Tauhardt, L., et al., *Linear Polyethyleneimine: Optimized Synthesis and Characterization – On the Way to "Pharmagrade" Batches.* Macromol Chem Phys, 2011. **212**(17): p. 1918-1924.
15. Bailey, F.E. and J.V. Koleske, *Poly(ethylene Oxide)*. 1976, New York, USA: Academic Press.
16. Graessley, W.W., G.S. Grest, and R.C. Hayward, *Excluded Volume Effects in Polymer Solutions: II. Comparison of Experimental Results with Numerical Simulation Data.* Macromolecules, 1999. **32**(10): p. 3510-3517.
17. Frenkel, D. and B. Smit, *Understanding Molecular Simulations*. 2nd ed. 2002, San Diego, USA: Academic Press.
18. Hallett, F.R., J. Watton, and P. Krygsman, *Vesicle sizing: Number distributions by dynamic light scattering.* Biophys J, 1991. **59**(2): p. 357-362.